Technical Report Documentation Page

1. Report No.	2. Government Accession No.	3. Recipient's Catalog No.
2022EF003409_pub		

4. Title and Subtitle	5. Report Date
Potential Impacts on Ozone and Climate From a Proposed Fleet of Supersonic Aircraft	March 2023
	6. Performing Organization Code

7. Author(s)	8. Performing Organization Report No.
Jun Zhang, Donald Wuebbles, Jens Holger Pfaender, Douglas Kinnison, and Nicholas Davis	

9. Performing Organization Name and Address	10. Work Unit No. (TRAIS)
Center of Excellence for: Alternative Jet Fuels and Environment University of Illinois, Urbana, IL, USA	11. Contract or Grant No. 13-C-AJFE-UI-029

12. Sponsoring Agency Name and Address	13. Type of Report and Period Covered
Federal Aviation Administration Office of Environment and Energy	Journal Article
	14. Sponsoring Agency Code

15. Supplementary Notes

16. Abstract

There has been renewed interest in developing commercial supersonic transport aircraft due to the increased overall demands by the public for air travel, the aspiration for more intercontinental travel, and the desire for shorter flight times. Various companies and academic institutions have been actively considering the designs of such supersonic aircraft. As these new designs are developed, the environmental impact on ozone and climate of these fleets need to be explored. This study examines one such proposed commercial supersonic fleet of 55-seater that is projected to fly at Mach 2.2, corresponding to cruise altitudes of 17–20 km, and which would burn 122.32 Tg of fuel and emit 1.78 Tg of NOx each year. Our analyses indicate this proposed fleet would cause a 0.74% reduction in global column ozone (~2 Dobson Units), which is mainly attributed to the large amounts of nitrogen oxides released in the atmosphere from the supersonic aircraft. The maximum ozone loss occurs at the tropics in the fall season, with a reduction of −1.4% in the total column ozone regionally. The stratospheric-adjusted radiative forcing on climate from this fleet was derived based on changes in atmospheric concentrations of ozone (59.5 mW/m 2), water vapor (10.1 mW/m 2), black carbon (−3.9 mW/m 2) and sulfate aerosols (−20.3 mW/m 2), resulting in a net non-CO2, non-contrail forcing of 45.4 mW/m 2, indicating an overall warming effect.

17. Key Words	18. Distribution Statement
ASCENT	

19. Security Classif. (of this report)	20. Security Classif. (of this page)	21. No. of Pages	22. Price
Unclassified	Unclassified		

Earth's Future

RESEARCH ARTICLE
10.1029/2022EF003409

Potential Impacts on Ozone and Climate From a Proposed Fleet of Supersonic Aircraft

Jun Zhang[1], Donald Wuebbles[2], Jens Holger Pfaender[3], Douglas Kinnison[1], and Nicholas Davis[1]

[1]National Center for Atmospheric Research, Boulder, CO, USA, [2]Department of Atmospheric Sciences, University of Illinois, Urbana, IL, USA, [3]School of Aerospace Engineering, Georgia Institute of Technology, Atlanta, GA, USA

Key Points:

- A proposed fleet of 55-seater supersonic aircraft is projected to fly at Mach 2.2 (17–21 km altitude) and burn 122.32 Tg of fuel each year and emit 1.78 Tg of NOx per year
- This proposed fleet would cause a 0.74% reduction in global column ozone (~2 Dobson Units), mainly attributed to the nitrogen oxides emissions
- Climate impact from changes in atmospheric ozone, water vapor and aerosols from this fleet result in a net non-CO_2 and non-contrail climate forcing of 45.4 mW/m^2

Supporting Information:

Supporting Information may be found in the online version of this article.

Correspondence to:

J. Zhang,
jzhan166@ucar.edu

Citation:

Zhang, J., Wuebbles, D., Pfaender, J. H., Kinnison, D., & Davis, N. (2023). Potential impacts on ozone and climate from a proposed fleet of supersonic aircraft. *Earth's Future*, *11*, e2022EF003409. https://doi.org/10.1029/2022EF003409

Received 6 DEC 2022
Accepted 15 MAR 2023

Abstract There has been renewed interest in developing commercial supersonic transport aircraft due to the increased overall demands by the public for air travel, the aspiration for more intercontinental travel, and the desire for shorter flight times. Various companies and academic institutions have been actively considering the designs of such supersonic aircraft. As these new designs are developed, the environmental impact on ozone and climate of these fleets need to be explored. This study examines one such proposed commercial supersonic fleet of 55-seater that is projected to fly at Mach 2.2, corresponding to cruise altitudes of 17–20 km, and which would burn 122.32 Tg of fuel and emit 1.78 Tg of NOx each year. Our analyses indicate this proposed fleet would cause a 0.74% reduction in global column ozone (~2 Dobson Units), which is mainly attributed to the large amounts of nitrogen oxides released in the atmosphere from the supersonic aircraft. The maximum ozone loss occurs at the tropics in the fall season, with a reduction of −1.4% in the total column ozone regionally. The stratospheric-adjusted radiative forcing on climate from this fleet was derived based on changes in atmospheric concentrations of ozone (59.5 mW/m^2), water vapor (10.1 mW/m^2), black carbon (−3.9 mW/m^2) and sulfate aerosols (−20.3 mW/m^2), resulting in a net non-CO_2, non-contrail forcing of 45.4 mW/m^2, indicating an overall warming effect.

Plain Language Summary With the general public's increased demand for air travel, a desire for more intercontinental travel with shorter flight times, there has been renewed interest in developing commercial supersonic transport aircraft. Various companies and academic institutions have been actively considering the design of such a supersonic aircraft. As these new designs are developed, the environmental impact of these realistic fleets on ozone and climate needs to be explored. This study looked at one such supersonic fleet, expected to fly at Mach 2.2, corresponding to a cruising altitude of 17–20 km, that would burn 122.32 Tg of fuel and emit 1.78 Tg of NOx per year. Our analysis shows that this proposed fleet would result in a 0.74% reduction in global columnar ozone (approximately 2 Dobson units), mainly due to the large atmospheric release of nitrogen oxides by supersonic aircraft. The impact on climate from this fleet was derived to have a net forcing of 45.4 mW/m^2, indicating an overall warming effect.

1. Introduction

The first commercial supersonic transport aircraft were first designed and built in the 1970s and consideration of such aircraft largely ceased in the late 1990s (e.g., Kawa et al., 1999; Penner et al., 1999). This perceived market has largely been left dormant since the retirement of the first commercial supersonic aircraft, the Concorde, in 2003. Environmental impacts associated with the operation of supersonic aircraft in the stratosphere have been an object of scientific interest since the 1970s (Grobecker et al., 1974) when the Concorde first entered into service.

There is now renewed interest in considering designs for supersonic commercial aircraft, especially for smaller passenger aircraft and for supersonic business jets (e.g., Carisosica et al., 2019). The expectation of aircraft designing, testing, and operating profitable, efficient, safety, and reliable supersonic civil aircraft have been greatly improved owning to the advancement in materials, propulsion, flight control technology, analytical methods, and performance prediction over the last four decades (MacIsaac & Langton, 2011; Nicolai & Carichner, 2010). With the recently renewed interest, various academic institutions and several companies have targeted the consideration of designs for supersonic transport aircraft, including actively developing new such aircraft (e.g., Boom, 2023; Eastham et al., 2022; Spike, 2023). Resulting environmental effects from fleets of these aircraft need to be evaluated.

Despite anticipated technical advancements, supersonic aircraft are still likely to have a greater environmental impact (in terms of noise and emissions) than their subsonic counterparts on a per-aircraft and per-passenger basis. Earlier studies have demonstrated the potential environmental effects of supersonic exhaust on stratospheric ozone abundance and on climate due to their burning of fossil-based aviation fuels (e.g., Cunnold et al., 1977; Grewe et al., 2007, 2010; Kawa et al., 1999; Pitari et al., 2004; Pitari & Mancini, 2001; Tie et al., 1994; Zhang et al., 2021a, 2021b). In the stratosphere, emissions of nitrogen oxides (NOx) can destroy ozone catalytically. Water vapor formed during fuel combustion provides a source of oxides of hydrogen (HOx) which can also destroy ozone. In addition, the sulfate and black carbon (BC) aerosols emission from the fuel combustion can provide more surface area density (SAD) for heterogeneous chemistry to occur on particles, which also leads to ozone destruction. Climate impacts result from changes in radiative forcing (RF). The largest contributors, in addition to the effects from direct emissions of carbon dioxide, have previously been identified to be the warming from emitted water vapor and cooling from sulfate aerosols (Grewe et al., 2007; Penner et al., 1999). Other contributions to RF occur from ozone production (warming) or destruction (cooling) and BC (warming). For these impacts, the higher cruise altitudes of supersonic aircraft are associated with increased atmospheric residence times for aircraft emissions, which increases the sensitivities of some atmospheric responses (Zhang et al., 2021a). Contrail impacts are not considered here, but we anticipate the effects from contrails would be negligible; lower stratospheric water vapor concentrations are very low (3–5 ppmv) and contrails in the stratosphere would not be expected to persist for very long.

Many prior studies have focused on examining the impacts of larger, high speed, high-flying commercial supersonic aircraft with rather long ranges, such as the major assessments (NASA assessment and Intergovernmental Panel for Climate Change special report on aviation). Their assessments of potential supersonic aircraft impacts were last conducted over 22 years ago, that largely examined a 300 passenger, Mach 2.4 aircraft design with cruise altitudes between 18 and 20 km and a range of 5,000 nmi (Kawa et al., 1999; Penner et al., 1999). In contrast, most of the supersonic aircraft designs currently under consideration are smaller and span a range of speeds and corresponding altitudes. For example, the Boom Overture design would operate at Mach 1.7 with cruise altitudes of 17–19 km and a capacity of 65–80 passengers (Boom, 2023).

Previous studies from Zhang et al. (2021a, 2021b) have revisited the ozone and climate impacts from a potential fleet of supersonic aircraft developed in 1990s, and then explored the sensitivity of atmospheric responses of ozone and climate from supersonic aircraft emissions at varying altitudes using the old emission inventory. As new aircraft designs and the corresponding fleet evaluations and emission inventory become available, there is a need to analyze the future environmental impact of such supersonic aircraft using state-of-the-art atmospheric chemistry-climate models. Eastham et al. (2022) has assessed the environmental impacts of a near-future supersonic aircraft fleet based on their proposed aircraft designs of a supersonic fleet flying at Mach 1.6 and 15–17 km altitude, burning 19 Tg of fuel each year and emitting 170 Gg of NOx. Their near-future supersonic aircraft fleet is assumed with current-generation engine technology burning fossil-based kerosene fuel and with current-day sulfur content. This study is aimed at examining the potential environmental impacts from the fleet for a newly proposed commercial supersonic aircraft design by the Aerospace Systems Design Laboratory (ASDL) at Georgia Tech (GT).

2. Aircraft Design and Emission Scenario for Supersonic Transport

The aircraft examined here was designed using the Framework for Advanced Supersonic Transport (FASST) (Baltman et al., 2022) developed at ASDL GT based on the Environmental Design Space (Kirby & Mavris, 2008) framework that initially was focused on purely subsonic commercial aircraft. FASST includes features specific to supersonic aircraft such as a more realistic modeling of the much tighter airframe, aerodynamics, and propulsion integration, as well as additional constraints over a much larger flight envelope, and supersonic inlets and nozzles. The focus here was on the larger commercial airline operated category instead of the smaller business jet category, due to the much larger market potential compared to the relatively small contributions of business jet operations.

Unlike many subsonic commercial transport aircraft studies, there are only one or two historic data points available to anchor conceptual design studies to realistic data. This is unfortunately insufficient to perform studies beyond those points by, for example, varying cruise Mach number or changes in materials or overall layout. Therefore, FASST uses well tested Computational Fluid Dynamics (CFD) capabilities such as the Euler-based

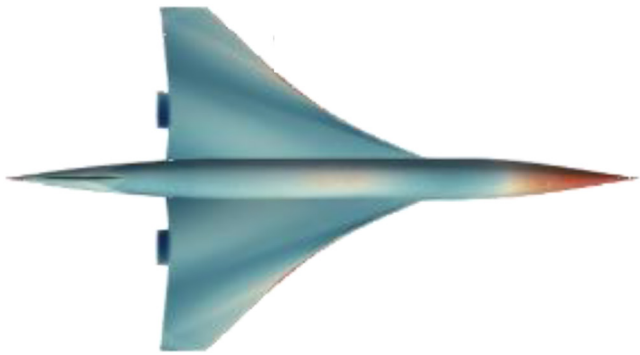

Figure 1. Top-Down View of the aircraft design with Mach Contours shown. Low surface Mach numbers are shown in orange/red. The absence of orange over the top of the wing and the aft fuselage indicates clean aero shaping avoiding unnecessary shocks which would increase wave drag and lower efficiency significantly.

CART3D (Aftosmis, 2020) with additional viscous corrections to predict the aircraft lift and drag. It is not currently computationally feasible to perform design studies using whole aircraft viscous CFD solutions for the entire flight envelope without a large super computing environment. Nevertheless, this approach represents a good compromise of resources and accuracy for early conceptual trade studies. After many iterations on the overall layout, the ASDL team converged on a four-engine, under-wing configuration with main wing integrated elevators and no horizontal tail or canards as control surfaces. The main fuselage is integrated with the wings, engines, and vertical tail and placed and shaped to achieve a shallow distribution of cross sections without steep gradients ("area-ruling") to minimize wave drag but keeping the passenger section sized for a two-class configuration with 1 + 1 and 2 + 1 seating for 55 passengers. The result is shown in Figure 1 and achieves a respectable lift-to-drag (L/D) ratio of 7.128, which while only slightly higher than Concorde (7 at Mach 2), is still respectable for the increased cruise Mach number.

The propulsion system was designed targeting an entry into service of roughly 2030 to 2035. FASST's propulsion capabilities are based on Numerical Propulsion System Simulation (Southwest Research Institute, link in reference) along with a number of additional software for component-specific performance and weight (Tong & Naylor, 2008; Wells et al., 2017). The selected engine architecture is a non-afterburning, two-spool, mixed-flow turbofan with low to medium bypass. The engine inlet, turbomachinery and nozzle were represented with parametric component maps while other components such as ducts, burner and mixer were represented with constant nominal loss metrics. The engine was sized using a multi-design point approach to simultaneously meet requirements at multiple flight conditions such as take-off, supersonic acceleration, and top of climb among others. While any new supersonic engine would most likely be based on one of the aircraft engine manufacturer's existing engine family cores, in order to significantly reduce development time and expense for a niche market, this study assumed a potential clean sheet design. Any engine based on existing cores will be forced to make certain trade-offs due to some mismatches in the requirements imposed by fitting an existing core to meet the thrust and temperature requirements of a supersonic transport engine. The resulting engine is superior to the Concorde engine and offers better thrust specific fuel consumption at the same Mach number and flight condition. The engine also delivers the required thrust without afterburning while also attempting to meet modern noise standards during take-off.

The routes with associated demand represent the expected upper limit for the total potential market for commercial supersonic operations in 2050 consisting of just over 2.35 million annual flights globally with the vehicle characteristics described previously. The number of flights translates into about 6800 supersonic commercial aircraft globally. Details on demand and routing derivation on this new fleet are illustrated in the supplementary Text S1 in the Supporting Information S1. A global overview with the optimized annual ground tracks is shown in Figure 2a. The aircraft are assumed to fly supersonically only over water (green lines in Figure 2a) due to concerns about noise from sonic booms in the over-populated regions. Figure 2b shows the accumulated fuel burn at different latitudes. In this scenario, about 85.9% of the emissions are assumed to take place in the Northern Hemisphere, with 36.4%, 45.6% and 3.8% in the northern tropics (0–30°N), mid-latitudes (30–60°N) and polar region (60–90°N). Compared to the emission scenario used in the earlier IPCC and NASA assessments, a larger fraction of emissions occurs near the tropics for this new supersonic fleet. The annual fuel consumption distribution as a function of altitude is shown in Figure 2c. The majority fuel are burnt between 17 and 21 km where the aircraft flying supersonically.

Conventional jet fuel was assumed to be used for the proposed supersonic aircraft. Emissions species included in this modeling study are NOx, H_2O, Sulfur dioxide (SO_2) and BC, listed in Table 1. Fuel usage and NOx amounts are calculated based on detailed engine state table-based emissions indices that were computed during the detailed engine analysis cycle which are based on supersonic combustor data (Niedzwiecki, 1992) from tests performed during the NASA High Speed Research program. The projected fuel burn and NOx emission are 122.32 Tg/yr and 1.78 Tg (NO_2)/yr respectively for this proposed fleet of supersonic aircraft, which gives a NO_2 emission index around 15 g/kg fuel burn. The emission index for water vapor is 1,237 g H_2O/kg fuel burned and therefore the corresponding total emissions for water vapor is equal to 151.31 Tg (H_2O)/yr. For comparison with

10.1029/2022EF003409

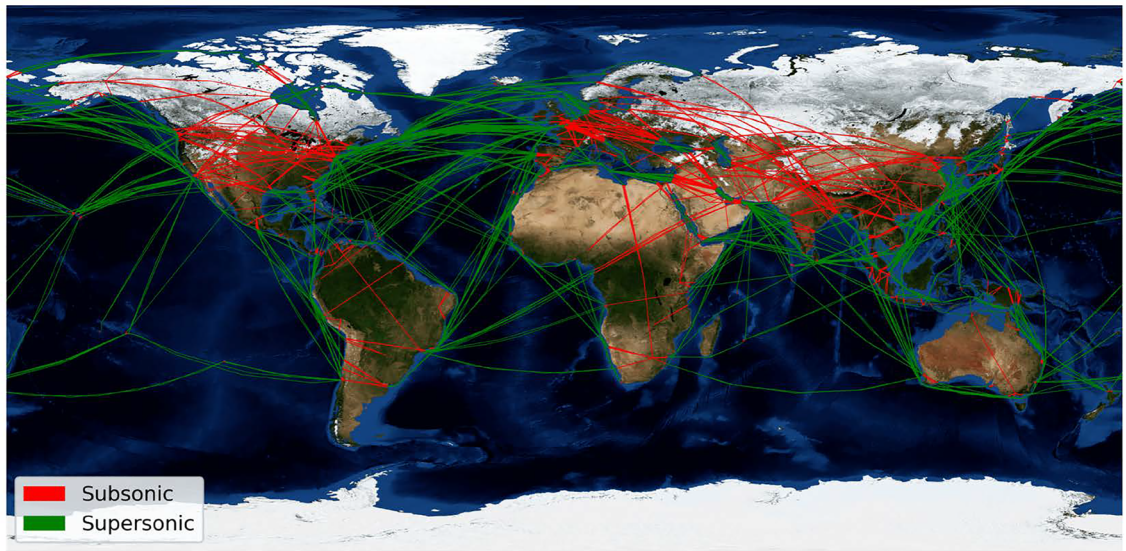

(a)

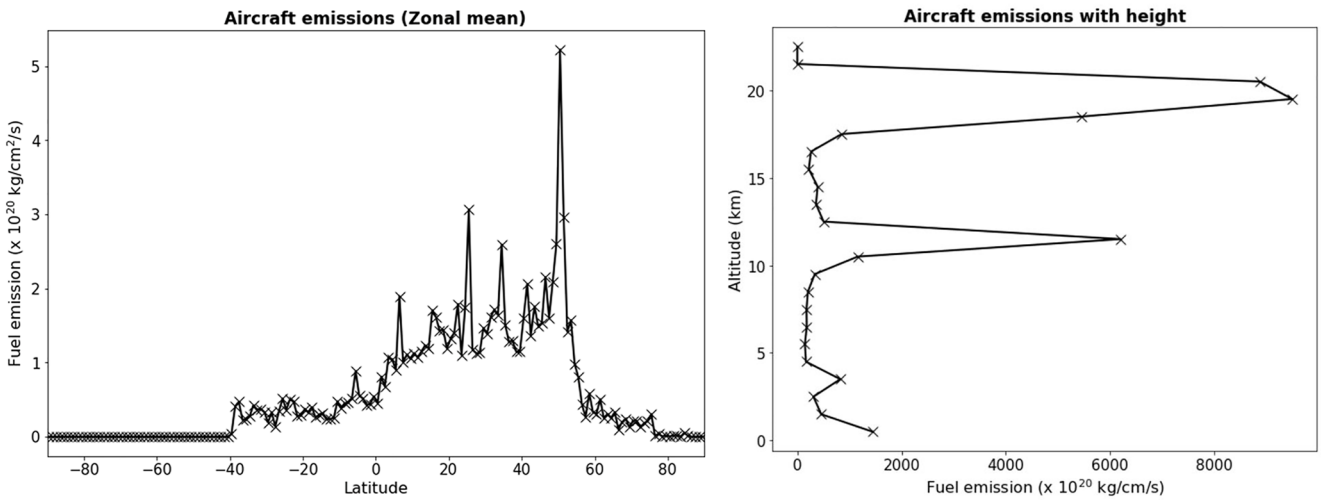

(b) (c)

Figure 2. (a) Projected annual global routes for the assumed fleet of supersonic aircraft. (b) Annually zonal mean vertically integrated fuel consumption as a function of latitude (kg/cm^2/s). (c) Annually fuel consumption as a function of altitude (kg/cm/s).

natural processes, the total natural atmospheric production of water vapor by methane oxidation and of nitrogen oxides by nitrous oxide oxidation calculated from D. Kinnison et al. (2020) are 60 Tg (H_2O)/yr and 2.8 Tg (NO_2)/yr, respectively. BC emission is proportional to the fuel burn and is assumed to be 0.05 g/kg fuel burn. The fuel sulfur concentration is assumed to be 600 mg/kg fuel burn.

Table 1
Emission Scenarios for the Proposed Fleet of Supersonic Aircraft

Mach number	Cruise altitude (km)	Fuel burn (Tg/yr)	NOx emission (Tg/yr)	H_2O emission (Tg/yr)	BC emission (Gg/yr)	Sulfur emission (Gg/yr)
2.2	17–21	122.32	1.78	151.31	6.12	73.39

3. Model Description and Simulations

The Community Earth System Model 2/Whole Atmosphere Community Climate Model version 6 (CESM2/WACCM6) was used to conduct the numerical experiments. This is the state-of-the-art coupled chemistry-climate model that includes comprehensive troposphere-stratosphere-mesosphere-lower-thermosphere chemistry from the Earth's surface to approximately 140 km (Gettelman et al., 2019). WACCM6 is a superset of the Community Atmosphere Model (CAM) version 6 (CAM6). WACCM6

includes all of the physical parameterizations of CAM6 plus the representation of parameterized gravity waves. It features a horizonal resolution of 0.9° latitude × 1.25° longitude using the finite volume dynamical core (Lin & Rood, 1997), and 70 vertical levels. The vertical resolution is ∼1.2 km in the lower stratosphere below 30 km, ∼2 km around the stratopause (∼50 km), and ∼3 km in the mesosphere and thermosphere. The vertical resolution in the troposphere is ∼1 km, except with higher resolution near the ground.

The chemistry package used in this study is troposphere, stratosphere, mesosphere and lower thermosphere (TSMLT, Tilmes et al., 2019), which contains the collection of reactions and species for the whole atmosphere. The species include all of the key source gases affecting the ozone chemistry, such as the extended O_x, NO_x, HO_x, ClO_x, and BrO_x chemical families. This chemical mechanism also includes methane and its degradation products, major source of NOx (N_2O), major source of HO_x (H_2O), as well as the various natural and anthropogenic precursors of the ClO_x and BrO_x families. In addition, this mechanism also includes primary nonmethane hydrocarbons and related oxygenated organic compounds. The chemical scheme is updated relative to the previous versions (e.g., Emmons et al., 2010; D. E. Kinnison et al., 2007; Lamarque et al., 2012; Marsh et al., 2013; Tilmes et al., 2016), with chemical kinetics and photochemical rate constants updated following JPL-2015 recommendations (Burkholder et al., 2015).

A total number of 231 species associated with 583 chemical reactions are included in the model, which breaks down into 150 photolysis reactions, 403 gas-phase reactions, 13 tropospheric, and 17 stratospheric heterogeneous reactions. The aerosol module used in WACCM6 is the four mode Modal Aerosol Model (MAM4, Liu et al., 2016). The aerosol SAD for the heterogeneous reactions is derived from MAM4 (Mills et al., 2016). The MAM4 has been updated to simulate the evolution of stratospheric sulfate aerosol from volcanic and supersonic aircraft emissions. In the stratosphere, the heterogenous reactions occur on three aerosol types—sulfate, nitric acid trihydrate and water ice. The liquid binary sulfate aerosol SAD is derived from MAM4 and updated using the Aerosol Physical Chemistry Model (Tabazadeh et al., 1994) in very cold regions (<200 K) to represent supercooled ternary solution aerosols. The solar variability, greenhouse abundances, reactive gases and aerosols from anthropogenic sources, biomass burning used in WACCM6 atmospheres are based on the Coupled Model Intercomparison Project Phase 6 (CMIP6) following the Shared Socioeconomic Pathways 2–4.5 (Eyring et al., 2016; Matthes et al., 2017; Meinshausen et al., 2017). This version of WACCM6 is being widely used in research studies and the results for the background atmosphere have been well evaluated relative to observations (e.g., Davis et al., 2021; Tilmes et al., 2019).

In this study, WACCM6 is run in a nudged, or specified dynamics (SD) configuration (WACCM6-SD), where the dynamics are relaxed to a free running simulation. There are two specified dynamics implementations in CESM2. In the older approach, the "SD" settings are configured to apply nudging only within the finite volume dynamical core as described in Kunz et al. (2011), with nudging targets calculated by a linear interpolation of the input meteorology to the current time. The second and new approach is an alternative dynamical-core-independent method that applies nudging as physics tendencies (described in Davis et al., 2022) with the nearest future input meteorology as the nudging target. This proactively pushes the modeled circulation toward the desired state. Here, we implement the second method and this study is the first study that applies and tests this new specified dynamics approach in WACCM6, which uses the alternative dynamical-core-independent method to apply nudging as physics tendencies. A free running Chemistry Climate Model Initiative (CCMI) simulation is used to generate high-frequency reference meteorology every 30-min dynamics timestep with a nudging timescale of 12 hr, which minimizes errors in tracers and tracer transport (Davis et al., 2022).

Two specified dynamics simulations are then performed for the supersonic aircraft study, whereby the winds and temperature are nudged toward the reference meteorology. The sea surface temperatures and sea ice used to drive the SD simulations are also derived from the existing CCMI simulation. Source gas boundary conditions used for the 2035 background atmospheres are based on the CMIP6. These two simulations are run for 12 years from 2025 to 2036, with one simulation including the supersonic aircraft emission and the other one excluding. Both SD simulations are driven with the same meteorology fields, kinetic reactions, heating rates, and climatology files, thus the difference between the two simulations are the changes induced from the supersonic aircraft emissions, excluding dynamics-chemical feedbacks.

We also use the PORT model (Conley et al., 2013), a configuration of the CAM in the CESM which runs the radiative transfer code offline. Using the same framework as CAM, PORT is able to reproduce the same heating rates and longwave and shortwave fluxes as those in CAM. PORT utilizes the radiation code from CAM

(Gent et al., 2011) and calculates the changes in stratospheric-adjusted RF under the fixed dynamical heating condition (Fels et al., 1980). PORT has been widely used and tested with CESM-generated datasets (e.g., Conley et al., 2013; Ivy et al., 2017; Lamarque et al., 2011; Polvani et al., 2020; Wang & Huang, 2020; Zhang et al., 2021a, 2021b), and have been implemented to calculate both instantaneous RF and RF including stratospheric temperature adjustment. We use PORT to estimate the stratospheric-adjusted RF attributable to the calculated changes in ozone, H_2O, BC, and sulfate.

4. Ozone Response to the Supersonic Transport Emission

The model derived changes in ozone from the supersonic fleet scenario is directly related to the emissions assumed, especially for the emissions of NOx, H_2O, BC, and SO_2, and the resulting changes in atmospheric concentrations of the gases and particles. Figure 3 shows the percentage change in the concentrations for these gases and particles by latitude and altitude as calculated from the difference between the simulations with and without the supersonic aircraft fleet emissions. The perturbations in total odd nitrogen are shown in Figure 3a (noted NOy and defined as the sum of $N + NO + NO_2 + NO_3 + 2N_2O_5 + HO_2NO_2 + HNO_3 + ClONO_2 +$ min or contributions from other nitrogen species; note that this includes the reactive nitrogen $NOx = NO + NO_2$ i.e., directly emitted into the atmosphere). Elevated NOy extends into the Southern Hemisphere (SH) with a larger fraction confined in the Northern Hemisphere (NH), corresponding to where the majority of emissions occur (86%). The enhancement peaks near 50°N (Figure S1b in the Supporting Information S1), which is collocated with the maximum emissions at 50°N. The percentage change of NOy depends on its background distribution (Figure S1a in the Supporting Information S1), resulting in the maximum percentage change of NOy near the NH tropics region around 10°N rather than 50°N (Figure 3a). The relative perturbation is largest (40%–80%) between 8 and 22 km at middle and high latitudes and from 15 to 25 km in the tropics (80%–160%).

Absolute changes in H_2O and BC show similar patterns in the NH as was found in NOy (Figure S1 in the Supporting Information S1), while the percentage changes of H_2O and BC show larger increase at higher altitudes as the H_2O and BC level drop sharply at higher stratosphere. Figure 3b shows the percentage increase in the water vapor concentration of the stratosphere resulting from the operation of the projected fleet. The largest perturbation (larger than 20%) in H_2O takes place between 30° and 60°N from 18 to 22 km, although the noticeable effect of the water emissions reaches the North Pole, the equator and even the SH. Distinct enhanced BC concentration is found throughout the stratosphere, with a maximum increase of more than 200% occurring at mid to high latitudes near cruise altitude. Supersonic emitted SO_2 is oxidized to the formation of sulfate aerosol (SO_4). The formed SO_4 aerosol increases the background level by more than 20% in the NH between 16 and 20 km.

Given that only 14% of the supersonic fleet emissions occur in the SH, a relatively large fraction of the material emitted by the aircraft's engines in the NH is transported and dispersed south of the equator. Compared to the supersonic emissions scenario used in the Zhang et al. (2021a, 2021b) studies, a larger fraction of emission is projected to occur near the tropics from the proposed fleet examined here. The strong upwelling that takes place in the tropics can lift emission from the lower or middle stratosphere to higher levels and then being transported across the equator.

The emissions of NOx, H_2O, BC and SO_2 from the assumed fleet of supersonic aircraft all have an influence on the resulting changes in ozone. The enhanced NOx and HOx (from H_2O emission) can both catalytically destroy ozone. In addition, the increased aerosols (BC and SO_4) can provide more SAD for heterogeneous chemistry to occur, which can also lead to ozone destruction.

The changes in odd oxygen ($Ox = O_3 + O + O(^1D)$ + other terms [e.g., Brasseur & Solomon, 2005; Wang et al., 1998]) is investigated to assess the perturbation in the chemical budget of odd oxygen as a function of altitude. The cycles incorporated in this study include the loss by NOx, HOx, and halogen oxides catalytic cycles (ClOx and BrOx, which are combined here to show interactions relative to the NOx and HOx cycles), as well as by the Chapman self-destruction cycle. The definition of Ox and the reactions included in each catalytic cycle are based on Brasseur and Solomon (2005) and can also be found in Text S2 in the Supporting Information S1. It has been established that the NOx involved Ox loss cycle (NOx−Ox) and HOx involved Ox loss cycle (HOx−Ox) both play important roles on the total Ox loss at different heights, with NOx−Ox between 30 and 40 km and HOx−Ox above 40 km, respectively (Bates & Nicolet, 1950; Crutzen, 1970, 1979). The loss from Ox self-loss cycle (Ox−Ox) and ClOx/BrOx involved Ox loss cycle (ClOx/BrOx−Ox) are important from 30 to 50 km, but

10.1029/2022EF003409

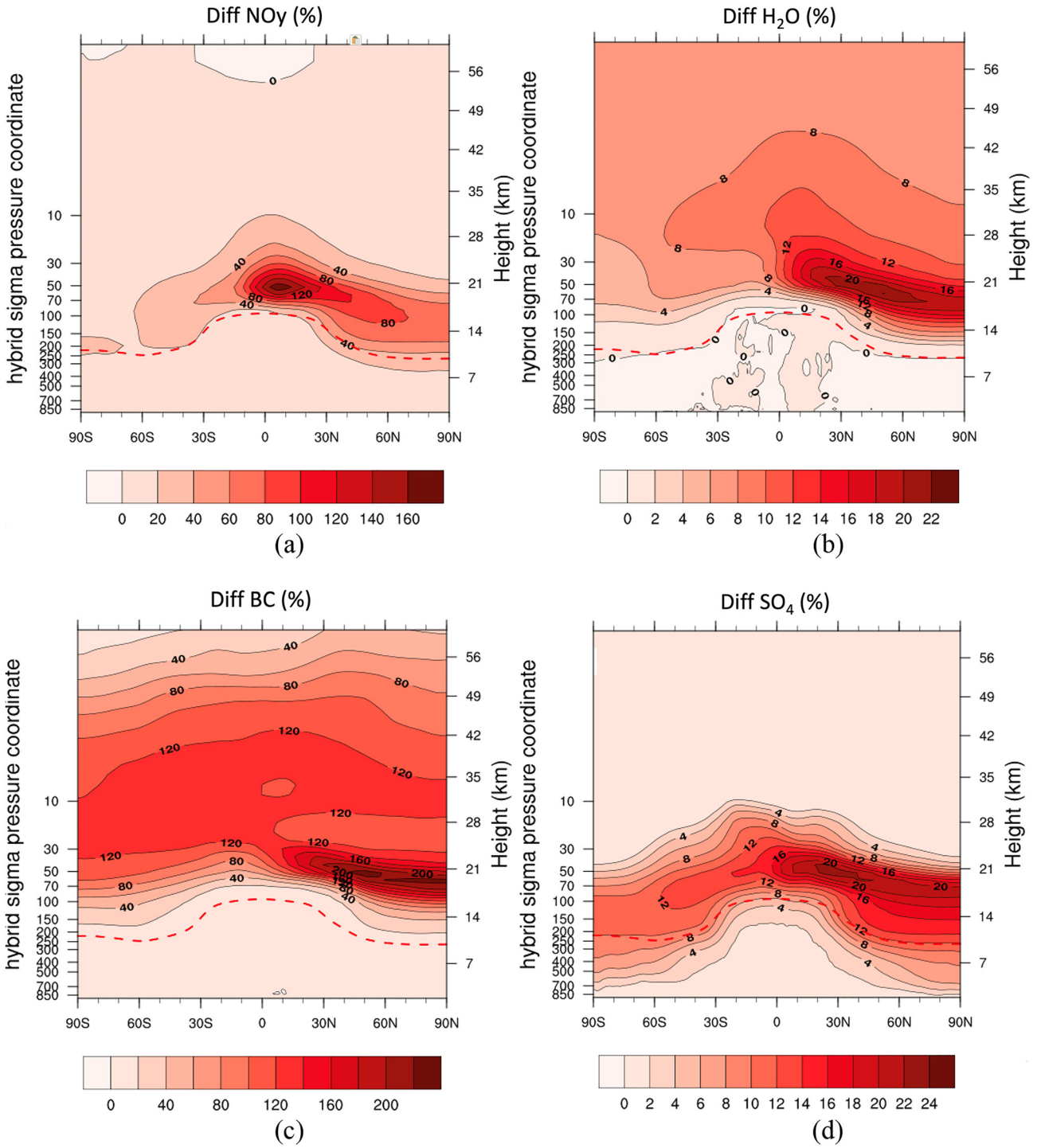

Figure 3. Calculated supersonic aircraft emission induced annually-averaged percentage change in the atmospheric mixing ratios of (a) NOy, (b) H_2O, (c) black carbon (BC) aerosol and (d) SO_4 aerosol. Cruise altitude is at 17–21 km. The red dashed line indicates the location of the lapse rate tropopause.

to a much less degree compared to NOx−Ox and HOx−Ox cycles. The NOx and H_2O emission from supersonic aircraft can direct perturb the NOx−Ox and HOx−Ox catalytic cycles in the background.

The rate of stratospheric ozone loss due to anthropogenic halogen emissions is also modulated by heterogeneous chemistry on volcanic aerosols in the stratosphere (Portmann et al., 1996; Solomon et al., 1996). Direct stratospheric BC and SO_2 emissions can substantially increase the aerosol SAD than nonvolcanic background values

in proposed fleet scenarios. A larger SAD provides more surfaces for heterogeneous chemistry to occur, which can perturb the halogen ClOx/BrOx involved Ox loss cycle. In this study, BC and SO_2 emissions can enhance the SAD by 10%–20% at the NH cruise altitudes (Figure S2 in the Supporting Information S1). In addition, the simultaneous release of NOx, H_2O, BC, and SO_2 compounds can lead to chemical interactions that could mitigate the effects of the individual emissions on ozone destruction. Thus, the consequences for stratospheric ozone changes depend on the interactions between emissions of nitrogen oxides, water vapor, aerosols, as well as chlorine and aerosol loadings of the atmosphere (Solomon et al., 1997; Weisenstein et al., 1998; World Meteorological Organization (WMO), 2018).

Figure 4a shows the annually zonal averaged percentage changes in ozone with height. A net production in ozone is found near the upper troposphere and lower stratosphere in both hemispheres. This ozone production extends to the surface except at the equator. Reduction of ozone is found in the middle to upper stratosphere and extends into the mesosphere. The maximum ozone depletion in percentage peaks over the tropical region at the 28–34 km with a reduction of −5%. This reduction extends southward to the SH and reaches the South Polar region, with a slightly larger fraction of ozone depletion confined in the NH. Compared to the results from Zhang et al. (2021a), where the ozone depletion maximizes in the NH high latitudes, the difference is due to the larger fraction of emission occurs at low to middle latitudes in this new projection. The mechanisms of the ozone destruction and production will be explored in Figures 5 and 6.

Total column ozone is the total amount of atmospheric ozone in a given column, and it is important in determining the overall exposure to harmful ultraviolet radiation at the Earth's surface. Total column ozone change is the net change in the sum of the ozone increase in the troposphere and lower stratosphere, and the ozone reduction in the middle and upper stratosphere shown in Figure 4a. Figure 4b shows the seasonal dependence of calculated percentage change in total column ozone with latitude. In the NH, total column ozone depletion occurs for the entire year, with a maximum of −1.4% loss appearing near tropics in late summer and early fall (August to October). In the SH, total column ozone shows an increase near mid-latitudes during September to April and polar regions in October and November. The SH maximum ozone depletion occurs in winter at high latitudes, which can potentially strengthen the Antarctic ozone hole. The annually averaged change in total column ozone with latitude and longitude is shown in Figure 4c, which suggests that the zonal pattern in ozone change due to supersonic emissions is instead dominated by ozone destruction in the mid to upper stratosphere. The emitted materials from the assumed fleet of supersonic aircraft would cause a reduction of −0.74% in global column ozone. Regionally, the maximum depletion reaches as much as −1.4% of total column ozone at the NH tropics near the Tibetan Plateau, while the earlier study indicates a maximum depletion at polar regions (Zhang et al., 2021a).

Figure 5 shows the annual averaged change in the different contributions to the Ox loss rate function of altitude at different latitude bands. Figures 5a, 5c, and 5e depict loss rates for the background atmosphere in percent of total Ox loss at 0–30°N, 30–60°N, and 60–90°N. In the stratosphere, HOx−Ox and NOx−Ox cycles play major roles in the total Ox loss, with much larger contributions than other two loss cycles (ClOx/BrOx−Ox and Ox−Ox) for three latitude bands. More than 70% of the background ozone loss results from the catalytic destruction by NOx at 28–32 km. HOx−Ox cycle contributes to more than 80% of ozone loss ranging from 8 to 19 km depending on latitude. At around 20 km where the cruise altitude planned for the assumed fleet, different loss rate is dominating the total loss at different latitude bands—with the HOx−Ox as the main loss for 0–30°N, 30–60°N, and equivalent contributions from HOx−Ox and NOx−Ox cycles at 60–90°N. At increasing latitudes, the NOx−Ox cycle becomes more important to the total loss in the lower stratosphere.

The supersonic aircraft-induced change at different latitudes is shown in Figures 5b, 5d, and 5f. As ozone is affected by the coupling of HOx, NOx and ClOx/BrOx chemistry, all the Ox chemical loss cycles are modified due to NOx, H_2O, BC and SO_2 emissions injected into the atmosphere. The vertical profile of total odd Ox loss shows the maximum loss occurs at around 30 km at 0–30°N and 30–60°N. While at higher latitude 60–90°N, there are two peaks for ozone depletion located at 20 and 35 km, respectively. Figure 5b indicates that the Ox loss is the greatest at 0–30°N among the three latitude bands investigated here. This loss is mainly attributed to the NOx−Ox cycle induced from the direct supersonic aircraft NOx emissions. The contribution of HOx-Ox loss to the total Ox loss is mainly in the upper stratosphere from 40 to 50 km, but to a much less extent compared to NOx−Ox loss at lower latitudes. At higher latitudes (60–90°N), the contribution of NOx−Ox and HOx-Ox loss cycles to total Ox total loss is more comparable.

The halogen involved Ox loss mainly occurs between 40–50 km and 10–20 km where the heterogeneous chemistry can be important at high latitudes. Figures 5b, 5d, and 5f indicate that halogen involved Ox loss overall

10.1029/2022EF003409

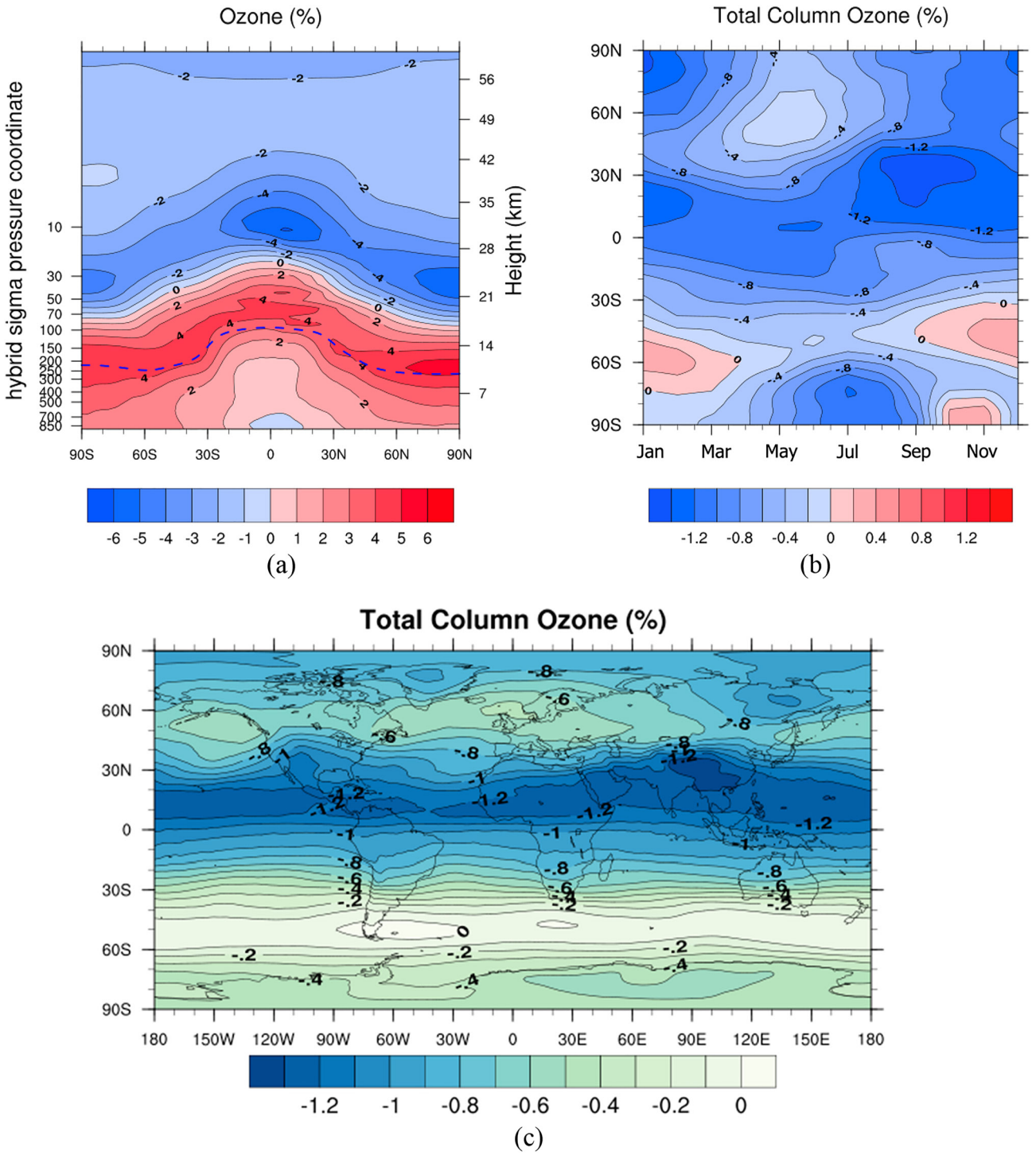

Figure 4. For the assumed supersonic aircraft fleet emissions, (a) the simulated annual and zonal mean perturbations (percent) in the atmospheric concentration of ozone at steady state; (b) Seasonal dependence of the calculated change in the total column ozone (%); (c) Annual average change in the total column ozone distribution (%).

plays a minor impact on total Ox loss at all latitude bands, which indicates that the increased SAD from BC and SO_2 emission has a minor impact on the overall ozone loss. This is mainly due to that the halogen-involved loss cycle is competing with other loss cycles at these altitudes where the Ox loss is dominated by the NOx emission. Additionally, the halogen involved Ox loss decreases between 10 and 40 km, which is due to the supersonic transport-induced NOx and HOx interfering with the halogen cycles by taking some of the reactive chlorine

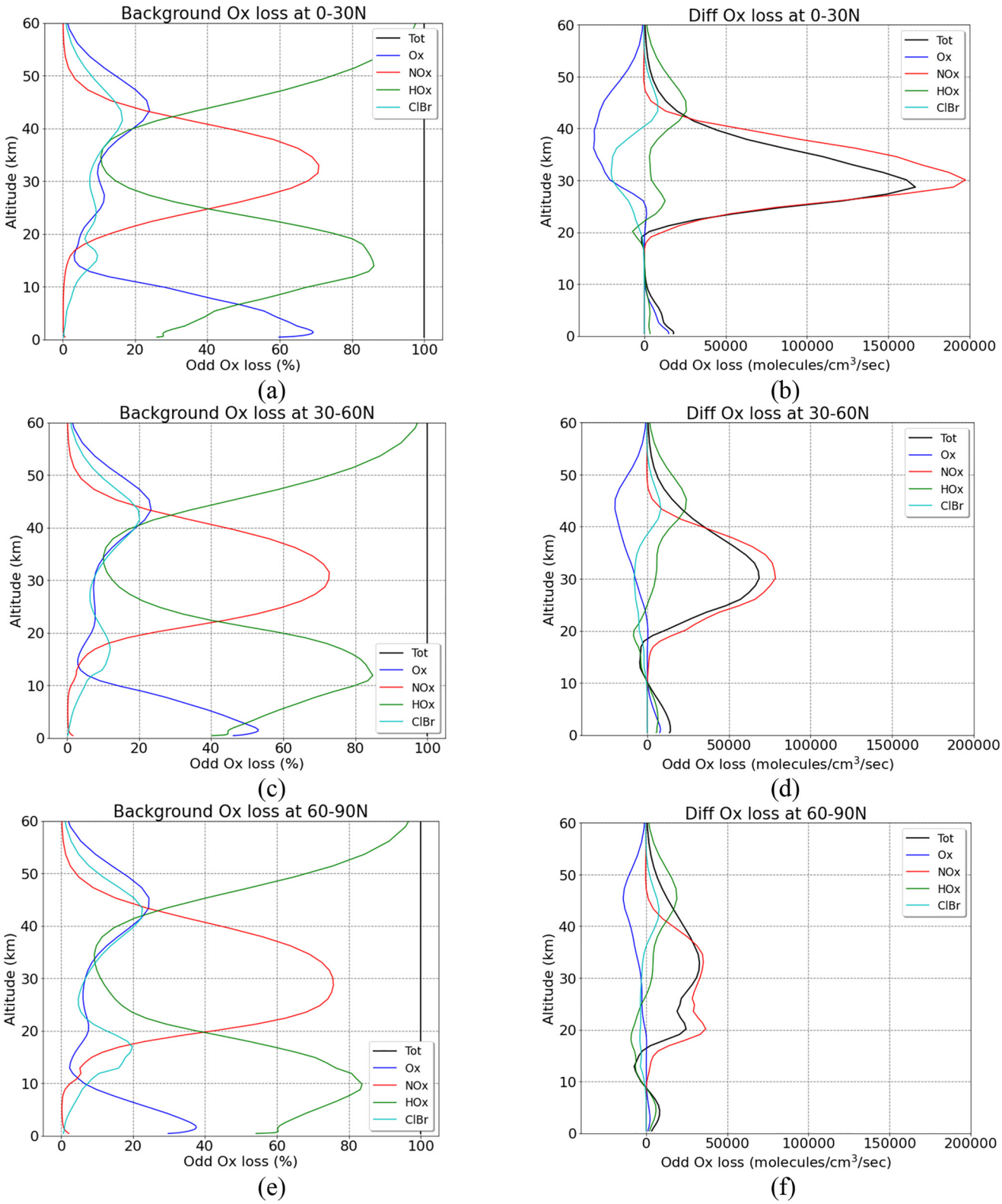

Figure 5. Annually profile of odd oxygen (Ox) chemical loss rates by catalytic cycles involving NOx, HOx and halogens as well as the chemical loss by the Chapman mechanism (Ox) for the background atmosphere at (a) 0–30°N; (c) 30–60°N; (e) 60–90°N. (b, d, and f) are the supersonic aircraft induced change (perturbation—background condition) at different latitudes.

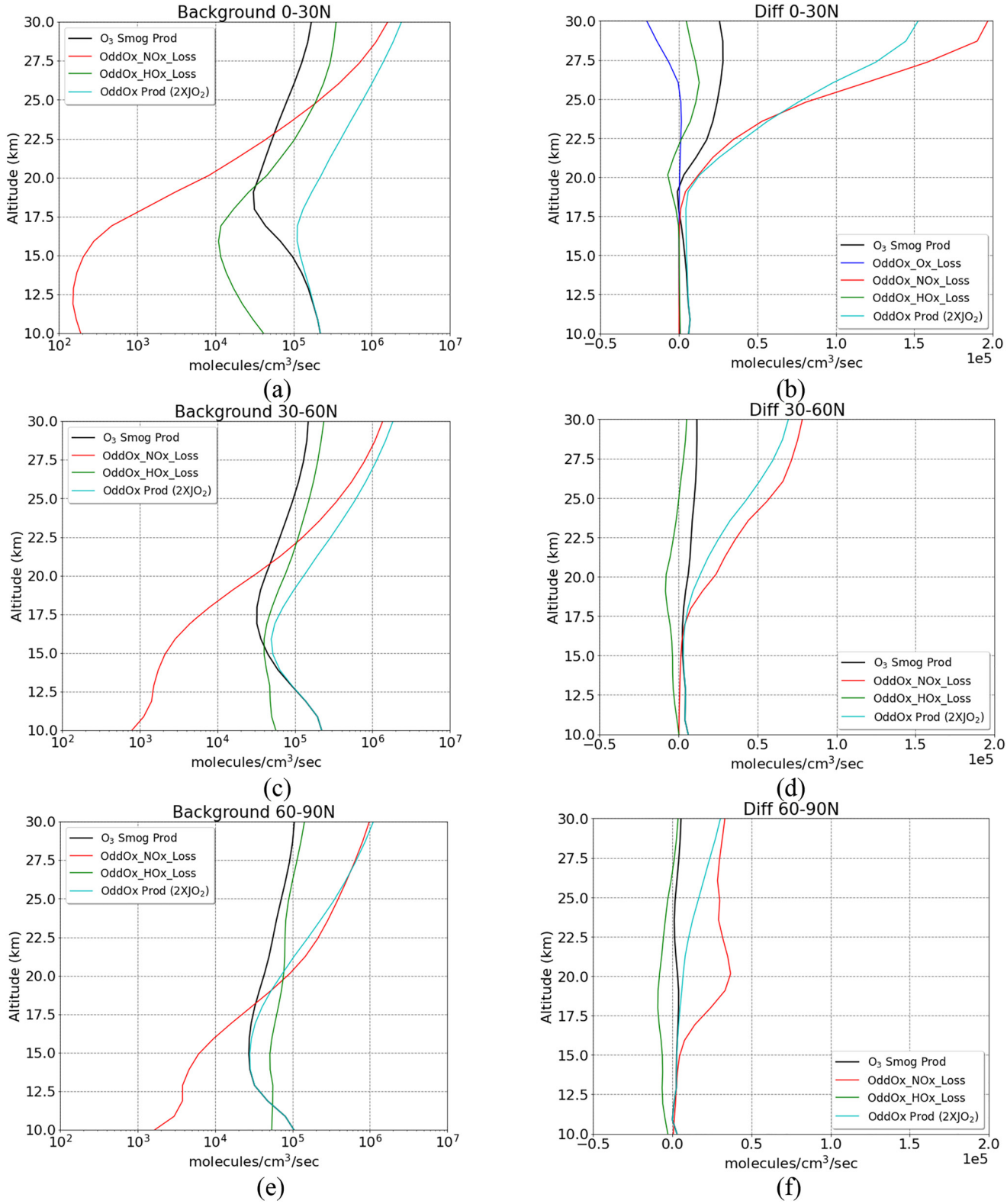

Figure 6. Background annual mean of ozone change due to smog chemistry (black line) O_3_smog_Prod = NO_HO_2 + CH_3O_2_NO + multiple NHMC_NO; total Ox product (blue line) 2 * JO_2 = O_2 + hv => 2O; NOx induced ozone loss (red line defined in Text S2 in the Supporting Information S1); HOx induced ozone loss (green line, defined in Text S2 in the Supporting Information S1) at (a) 0–30°N; (c) 30–60°N; (e) 60–90°N. (b, d, and f) are the supersonic aircraft induced change.

and bromine and converting them into the relatively less reactive reservoirs (e.g., $ClONO_2$). Odd-oxygen loss (Ox−Ox) decreases in the stratosphere at all latitudes. With the additional perturbation from supersonic aircraft emission, more Ox is destroyed by the NOx-Ox and/or HOx-Ox loss cycles, leading to the reduction of Ox-Ox loss at the same location.

The discussion here mainly considers the direct chemical impact on stratospheric ozone. Emissions of NOx, H_2O, BC and SO_2 can potentially interact with stratospheric ozone through the stratospheric temperature and dynamics feedbacks. BC can absorb solar radiation and emit heat, which leads to temperature increase and further influence the loss rate of ozone destroying reactions (WMO, 2018). In addition, changing in stratospheric temperature can shift stratospheric dynamics, which will further alter stratospheric ozone concentration. Since the specified dynamics approach is applied in this study, the feedback effects resulting from chemical-dynamical interactions are not taken into account in the results shown here. D. Kinnison et al. (2020) has done a coupled study that has incorporated the chemical and dynamical interactions, but for hypersonic aircraft where the fleet emissions occur at a much higher altitude (∼30 km). They show a temperature decrease at the cruise altitude due to the ozone depletion. The resulted ozone change is qualitatively the same between specified dynamics and coupled simulations, while quantitatively the maximum ozone depletion is reduced by about a third due to the chemistry and temperature feedback in the stratosphere. We anticipate the effect would be smaller in our case because of the emissions being at a lot lower altitude, while further coupled simulations need to be performed to find out the magnitude of the changes.

Figure 6 investigates the mechanism causing the ozone increase in the troposphere and lower stratosphere (Figure 4a) at different latitudes. The ozone increase in this region can be attributed to multiple processes: (a) the direct effects of enhanced ozone production from NOx emissions (smog-like chemistry); (b) the ozone self-healing effect resulting from the ozone depletion at higher altitudes; (c) a decrease in the ozone loss rates in this region due to the interference of the emitted NOx with the HOx ozone loss cycle; (d) through a combination of previous three processes. Figures 6a, 6c, and 6e show the background annual mean of ozone change due to the three mechanisms at different latitude bands—smog chemistry production, total Odd Ox production, as well as the Ox loss rate due to the NOx and HOx family cycles. The net ozone change near tropopause is modulated by ozone production and destruction processes. HOx-induced ozone loss plays a major role in total loss at the upper troposphere and lower stratosphere region. NOx-induced ozone loss surpasses the NOx-induced ozone production at around 25, 22 and 20 km at 0–30°N, 30–60°N, 60–90°N, respectively, which is due to the NOx-induced ozone loss increases at higher latitude. Smog chemistry production and total Odd Ox production are the strongest at 0–30°N owing to stronger sunlight exposure near tropics.

The supersonic aircraft emission-induced changes are shown in Figures 6b, 6d, and 6f. The mechanism causing the ozone increase near tropopause is different at each latitude band. In the tropics, the ozone increase can be attributed to smog chemistry production and total Odd Ox production (Figure 6b). At middle latitude, the combination of smog chemistry production, total Odd Ox production and reduced ozone loss from HOx−Ox cycle are responsible for the ozone increase. The reduced HOx−Ox loss rate is playing a more important role in the polar region, because of less solar ultraviolet light at high latitudes (Figure 6f). The decrease in the HOx−Ox loss rate is attributed to the NOx emission. Emissions from a fleet of supersonic aircraft results in perturbations of the catalytic ozone destruction cycles by causing a repartitioning between the chemical families.

5. Radiative Forcing Response to the Supersonic Transport Emission

While the climate effects, including the effects on surface temperature, precipitation, and severe weather, are too small to be directly evaluated for this fleet of supersonic aircraft, we can evaluate the RF on climate from the proposed fleets of supersonic aircraft. Normally, the Earth maintains nearly a radiative balance between solar heating and the cooling from terrestrial infrared radiation that escapes to space. When a particular human activity changes greenhouse gas concentrations, particles, or land albedo, this results in a radiative imbalance. Radiative forcing (RF in W/m^2) is the measure of the change in energy balance as a result of a change in a forcing agent (e.g., greenhouse gaseous, aerosol, cloud, and surface albedo) that effects the global energy balance and contributes to climate change (Finlayson-Pitts & Pitts, 1999).

In this study, we quantify the changes in RF associated with the assumed supersonic aviation emissions of H_2O, NOx, SO_2, and BC. A rough calculation of CO_2 impact indicates that the year's fuel usage from the assumed

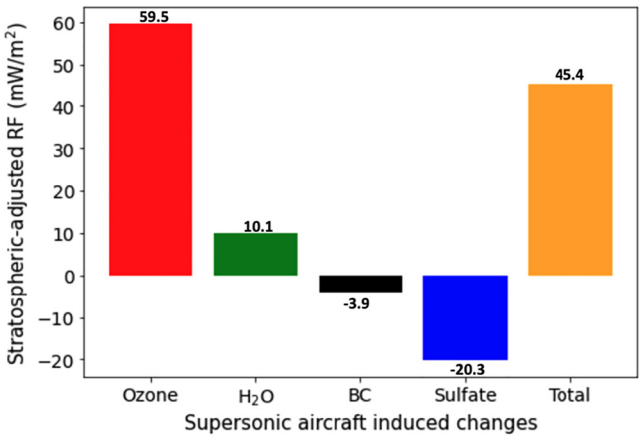

Figure 7. Annual and global average change in stratospheric-adjusted radiative forcing (mW/m^2) at the tropopause for supersonic aircraft induced changes in ozone, H_2O, black carbon and sulfate.

fleet implies an additional 386 Tg CO_2 emission. Using 5.148×10^{18} kg as the mass of the atmosphere (Trenberth & Smith, 2005), 1 ppm of CO_2 has a mass of 7.821×10^{12} kg. The additional 386 Tg CO_2 can induce the increase of atmospheric CO_2 0.050 ppmv, with a RF of 0.819 mW/m^2. Previous studies have indicated that the contribution to global climate change from stratospheric ozone and water vapor perturbations is likely larger than that from CO_2 emission (Penner et al., 1999; Zhang et al., 2021a, 2021b), so we focus on evaluating non-CO_2, non-contrail climate forcing of a near-future supersonic aircraft fleet. For the assumed aviation fleet perturbations to H_2O, ozone, BC and sulfate, the atmospheric response should reach a steady state in less than a decade, and thus the climate impacts can be evaluated based on the instantaneous fleet size.

Supersonic aircraft H_2O, NOx, SO_2, and BC emissions can affect the climate both directly and indirectly. The H_2O released in the stratosphere is a strong greenhouse gas which will warm the surface while cooling the stratosphere. This enhanced stratospheric H_2O has much higher warming efficacy than the H_2O released in the troposphere since the small perturbation in tropospheric H_2O gets removed quickly by precipitation (Brasseur et al., 2016; Lee et al., 2010). The SO_2 becomes stratospheric sulfate particles. Stratospheric sulfate (scatterers) and BC (absorbers) intercept solar radiation cooling the surface while warming the stratosphere. All the emission species can perturb stratospheric ozone and affect the climate indirectly. The chemically induced ozone decrease in the stratosphere will cool both the surface and the stratosphere.

RF calculations are performed using the PORT model with the WACCM derived changes in ozone, H_2O, BC and sulfate. When the radiative perturbation occurs above the tropopause in the stratosphere as for the supersonic aircraft impacts, this perturbation is not rapidly transported into the troposphere. This radiative imbalance will lead to changes in local temperature that restores the radiative balance within the stratosphere. Such changes in stratospheric temperature will alter the tropospheric radiation and lead to a warmer or cooler climate system. The RF calculation that incorporated the adjustment of stratospheric temperatures is denoted "stratosphere-adjusted RF." All RF values in this study are calculated with "stratospheric adjustment" which allows stratospheric temperatures to reach radiative equilibrium using a fixed dynamical heating assumption (Fels et al., 1980).

The calculated annual average change in stratospheric-adjusted RF for supersonic aircraft -induced changes in Ozone, H_2O, BC and Sulfate are shown in Figure 7. For the new proposed fleets of supersonic aircraft, the ozone and H_2O perturbations are calculated to have a warming effect with an RF of 59.5 and 10.1 mW/m^2, respectively. For BC and Sulfate perturbations, the RFs are −3.9 and −20.3 mW/m^2, respectively, denoting a cooling effect at the surface. Combined the effects from perturbations of all species, we find a net positive RF of 45.4 mW/m^2. This number is comparable to the RF of 57.4 mW/m^2 induced by contrail cirrus from all the subsonic aircraft operated in 2018 (Lee et al., 2020). We acknowledge that the regional patterns of RF may differ for each species, but we take their summed RF as a first-order measure of the global mean impact.

6. Discussion and Conclusions

Using a new emission scenario of a proposed fleet of supersonic aircraft targeting an entry into service of roughly 2030 to 2035, our study investigated the potential atmospheric impacts of this realistic near-term supersonic designs. The state-of-the-art whole atmosphere chemistry-climate model, WACCM, coupled with the latest specified dynamics scheme, was used to assess impacts on atmospheric ozone and non-CO_2 and non-contrail climate forcings. This new proposed fleet supersonic fleet is projected to fly at Mach 2.2 and 17–21 km altitude, which burns 122.32 Tg of fuel each year and emitting 1.78 Tg of NOx. The aircraft designs and emission scenarios proposed in this study are quite different from a study done by Eastham et al. (2022) for a different supersonic fleet. In their study, they proposed a fleet of supersonic aircraft flying at Mach 1.6 and 15–17 km altitude, burning 19 Tg of fuel each year and emitting 170 Gg of NOx. The fuel burn and NOx emission projected in this study are about 6 and 10 times larger than the projections in Eastham et al. (2022), respectively.

As shown by the model simulations presented here, we found the proposed fleet of supersonic aircraft can cause a 0.74% reduction in global column ozone, which is around 2 Dobson Units of global ozone depletion, equivalent

to 20% of the total impact of chlorofluorocarbon emissions at their peak. This ozone depletion is mainly attributed to the large amounts of direct nitrogen oxides emissions. The impacts of water vapor and SO_2 on the ozone column is found to be smaller. The maximum ozone loss occurs in the NH tropics in the fall season, with a local reduction of −1.4% in total column ozone. The ozone reduction calculated in our study is more than 10 times higher than the estimation from Eastham et al. (2022), where they calculated a reduction of 0.046% in global column ozone. This 10 times difference is consistent with the NOx emission used in our study (1.78 Tg) and Eastham et al. (2022) study (170 Gg), owning to different assumptions of travel demands and aircraft designs.

We assess the ozone increase in the upper troposphere and lower stratosphere and ozone decrease in the middle to upper stratosphere in different latitude bands. In the tropics, the ozone increase is attributed to smog chemistry production and total Odd Ox production; in middle latitudes, the combination of smog chemistry production, total Odd Ox production and reduced ozone loss from the HOx−Ox cycle are responsible for the ozone increase; in the polar region, the reduced HOx−Ox loss rate is playing a more important role. In terms of climate impact of this proposed fleet of supersonic aircraft, the stratospheric-adjusted RF was estimated from changes in atmospheric concentrations of ozone (59.5 mW/m^2), water vapor (10.1 mW/m^2), BC (−3.9 mW/m^2) and sulfate aerosols (−20.3 mW/m^2), resulting in a net non-CO_2, non-contrail forcing of 45.4 mW/m^2, indicating an overall warming effect. While in Eastham et al. (2022), they estimated the net RF from non-CO_2, non-contrail forcing of −3.5 mW/m^2, varying from −3.0 to −3.9 mW/m^2 year to year, which indicates an overall cooling effect.

The atmospheric impacts of any proposed fleet of supersonic aircraft need to be fully examined and understood before putting these aircraft into operation. Some assumptions in this study can contribute to uncertainties. For example, the background atmosphere is assumed to be under volcanic clean conditions in the 2035 time period. The ozone depletion could be larger if emissions occurred during a major volcanic eruption, which would accelerate heterogenous chemistry. We also do not consider plume chemistry in this study, which can be important in the initial plume if comparing with the well-mixed case at short time intervals. The dynamical effects due to local heating by BC and ozone changes are also not included, which could force circulation feedbacks that alter transport. Heating in the tropics could accelerate the Brewer-Dobson circulation, which would flux more ozone to the pole. Further work will be needed to reduce the uncertainties and to evaluate effects which are not considered here.

Data Availability Statement

The emission inventory and atmospheric modeling datasets used in this study are available to the community through the Illinois Data Bank (IDB), a public access repository at the University of Illinois Urbana-Champaign, link https://databank.illinois.edu/datasets/IDB-0038951.

Acknowledgments
This work is supported by Grant AGS-1906719 from the Atmospheric Chemistry Observation & Modeling lab of the U.S. National Science Foundation (NSF). This material is based upon work supported by National Center for Atmospheric Research (NCAR), which is a major facility sponsored by NSF under the Cooperative Agreement 1852977. The University of Illinois received support from the U.S. Federal Aviation Administration (13-C-AJFE-UI-029).

References

Aftosmis, M. J. (2020). Cart3D. https://www.nas.nasa.gov/publications/software/docs/cart3d/. Last update October, 2020.

Baltman, E., Tai, J., Ahuja, J., Stewart, B., Perron, C., De Azevedo, J., et al. (2022). A methodology for determining the interdependence of fuel burn and LTO noise of a commercial supersonic transport. AIAA 2022-4110. *AIAA AVIATION 2022 Forum*. https://doi.org/10.2514/6.2022-4110

Bates, D. R., & Nicolet, M. (1950). The photochemistry of atmospheric water vapor. *Journal of Geophysical Research*, *55*(3), 301–327. https://doi.org/10.1029/JZ055i003p00301

Boom. (2023). Overture. Retrieved from https://boomsupersonic.com/overture

Brasseur, G. P., & Solomon, S. (2005). *Aeronomy of the middle atmosphere*. In *Atmospheric and Oceanographic Science Library* (Vol. 32). Springer.

Brasseur, G. P., Gupta, M., Anderson, B. E., Balasubramanian, S., Barrett, S., Duda, D., et al. (2016). Impact of aviation on climate: FAA's aviation climate change research initiative (ACCRI) phase II. *Bulletin of the American Meteorological Society*, *97*(4), 561–583. https://doi.org/10.1175/BAMS-D-13-00089.1

Burkholder, J. B., Sander, S. P., Abbatt, J. P. D., Barker, J. R., Huie, R. E., Kolb, C. E., et al. (2015). *Chemical kinetics and photochemical data for use in atmospheric studies: Evaluation number 18*. Technical Report. Jet Propulsion Laboratory, National Aeronautics and Space Administration.

Carisosica, S. A., Lock, J. W., Boyd, I. D., Lewis, M. J., & Hallion, R. P. (2019). *Commercial development of civilian supersonic aircraft*. IDA Document D-10845. IDA Science and Tecnology Policy Institute. Retrieved from https://www.ida.org/-/media/feature/publications/c/co/commercial-development-of-civilian-supersonic-aircraft/d-10845.ashx

Conley, A. J., Lamarque, J. F., Vitt, F., Collins, W. D., & Kiehl, J. (2013). PORT, a CESM tool for the diagnosis of radiative forcing. *Geoscientific Model Development*, *6*(2), 469–476. https://doi.org/10.5194/gmd-6-469-2013

Crutzen, P. J. (1970). The influence of nitrogen oxides on the atmospheric ozone content. *Quarterly Journal of the Royal Meteorological Society*, *96*(408), 320–325. https://doi.org/10.1002/qj.49709640815

Crutzen, P. J. (1979). The role of NO and NO2 in the chemistry of the troposphere and stratosphere. *Annual Review of Earth and Planetary Sciences*, *7*(1), 443–472. https://doi.org/10.1146/annurev.ea.07.050179.002303

Cunnold, D. M., Alyea, F. N., & Prinn, R. G. (1977). Relative effects on atmospheric ozone of latitude and altitude of supersonic flight. *AIAA Journal*, *15*(3), 337–345. https://doi.org/10.2514/3.7327

Davis, N. A., Callaghan, P., Simpson, I. R., & Tilmes, S. (2022). Specified dynamics scheme impacts on wave-mean flow dynamics, convection, and tracer transport in CESM2 (WACCM6). *Atmospheric Chemistry and Physics*, *22*(1), 197–214. https://doi.org/10.5194/acp-22-197-2022

Davis, N. A., Richter, J. H., Edwards, J., & Glanville, A. A. (2021). A positive zonal wind feedback on sudden stratospheric warming development revealed by CESM2 (WACCM6) reforecasts. *Geophysical Research Letters*, *48*(5), e2020GL090863. https://doi.org/10.1029/2020GL090863

Eastham, S. D., Fritz, T., Sanz-Morère, I., Prashanth, P., Allroggen, F., Prinn, R. G., et al. (2022). Impacts of a near-future supersonic aircraft fleet on atmospheric composition and climate. *Environmental Science: Atmospheres*, *2*(3), 388–403. https://doi.org/10.1039/D1EA00081K

Emmons, L. K., Walters, S., Hess, P. G., Lamarque, J.-F., Pfister, G. G., Fillmore, D., et al. (2010). Description and evaluation of the model for ozone and related chemical Tracers, version 4 (MOZART-4). *Geoscientific Model Development*, *3*(1), 43–67. https://doi.org/10.5194/gmd-3-43-2010

Eyring, V., Bony, S., Meehl, G. A., Senior, C. A., Stevens, B., Stouffer, R. J., & Taylor, K. E. (2016). Overview of the coupled model inter-comparison project phase 6 (CMIP6) experimental design and organization. *Geoscientific Model Development*, *9*(5), 1937–1958. https://doi.org/10.5194/gmd-9-1937-2016

Fels, S. B., Mahlman, J. D., Schwarzkopf, M. D., & Sinclair, R. W. (1980). Stratospheric sensitivity to perturbations in ozone and carbon dioxide: Radiative and dynamical response. *Journal of the Atmospheric Sciences*, *37*(10), 2265–2297. https://doi.org/10.1175/1520-0469(1980)037<2265:SSTPIO>2.0.CO;2

Finlayson-Pitts, B. J., & Pitts, J. N., Jr. (1999). *Chemistry of the upper and lower atmosphere: Theory, experiments, and applications*. Elsevier.

Gent, P. R., Danabasoglu, G., Donner, L. J., Holland, M. M., Hunke, E. C., Jayne, S. R., et al. (2011). The community climate system model version 4. *Journal of Climate*, *24*(19), 4973–4991. https://doi.org/10.1175/2011JCLI4083.1

Gettelman, A., Mills, M. J., Kinnison, D. E., Garcia, R. R., Smith, A. K., Marsh, D. R., et al. (2019). The whole atmosphere community climate model version 6 (WACCM6). *Journal of Geophysical Research: Atmospheres*, *124*(23), 12380–12403. https://doi.org/10.1029/2019JD030943

Grewe, V., Plohr, M., Cerino, G., Di Muzio, M., Deremaux, Y., Galerneau, M., et al. (2010). Estimates of the climate impact of future small-scale supersonic transport aircraft–results from the HISAC EU-project. *Aeronautical Journal*, *114*(1153), 199–206. https://doi.org/10.1017/s000192400000364x

Grewe, V., Stenke, A., Ponater, M., Sausen, R., Pitari, G., Iachetti, D., et al. (2007). Climate impact of supersonic air traffic: An approach to optimize a potential future supersonic fleet–results from the EU-project SCENIC. *Atmospheric Chemistry and Physics*, *7*(19), 5129–5145. https://doi.org/10.5194/acp-7-5129-2007

Grobecker, A. J., Coroniti, S. C., & Cannon, R. H. (1974). *The effects of strato- spheric pollution by aircraft*. Technical Report DOT-TST-75-50. Department of Transportation.

Ivy, D. J., Hilgenbrink, C., Kinnison, D., Alan Plumb, R., Sheshadri, A., Solomon, S., & Thompson, D. W. (2017). Observed changes in the Southern Hemispheric circulation in May. *Journal of Climate*, *30*(2), 527–536. https://doi.org/10.1175/JCLI-D-16-0394.1

Kawa, S. R., Anderson, J. G., Baughcum, S. L., Brock, C. A., Brune, W. H., Cohen, R. C., et al. (1999). Assessment of the effects of high-speed aircraft in the stratosphere: 1998. National Aeronautics and Space Administration report. NASA/TMM1999-209237.

Kinnison, D., Brasseur, G., Baughcum, S. L., Zhang, J., & Wuebbles, D. (2020). The impact on the ozone layer of a potential fleet of civil hypersonic aircraft. *Earth's Future*, *8*(10), e2020EF001626. https://doi.org/10.1029/2020EF001626

Kinnison, D. E., Brasseur, G. P., Walters, S., Garcia, R. R., Marsh, D. R., Sassi, F., et al. (2007). Sensitivity of chemical tracers to meteorological parameters in the MOZART-3 chemical transport model. *Journal of Geophysical Research*, *112*(D20), D20302. https://doi.org/10.1029/2006JD007879

Kirby, M. R., & Mavris, D. N. (2008). The environmental design space. In *26th international congress of the aeronautical sciences ICAS* (pp. 1–9). Retrieved from https://www.icas.org/ICAS_ARCHIVE/ICAS2008/PAPERS/586.PDF

Kunz, A., Pan, L. L., Konopka, P., Kinnison, D. E., & Tilmes, S. (2011). Chemical and dynamical discontinuity at the extratropical tropopause based on START08 and WACCM analyses. *Journal of Geophysical Research*, *116*(D24), D24302. https://doi.org/10.1029/2011JD016686

Lamarque, J.-F., Emmons, L. K., Hess, P. G., Kinnison, D. E., Tilmes, S., Vitt, F., et al. (2012). CAM-chem: Description and evaluation of interactive atmospheric chemistry in the Community Earth System Model. *Geoscientific Model Development*, *5*(2), 369–411. https://doi.org/10.5194/gmd-5-369-2012

Lamarque, J.-F., Kyle, G. P., Meinshausen, M., Riahi, K., Smith, S. J., van Vuuren, D. P., et al. (2011). Global and regional evolution of short-lived radiatively-active gases and aerosols in the representative concentration pathways. *Climatic Change*, *109*(1–2), 191–212. https://doi.org/10.1007/s10584-011-0155-0

Lee, D. S., Fahey, D. W., Skowron, A., Allen, M. R., Burkhardt, U., Chen, Q., et al. (2020). The contribution of global aviation to anthropogenic climate forcing for 2000 to 2018. *Atmospheric Environment*, *244*, 117834. https://doi.org/10.1016/j.atmosenv.2020.117834

Lee, D. S., Pitari, G., Grewe, V., Gierens, K., Penner, J. E., Petzold, A., et al. (2010). Transport impacts on atmosphere and climate: Aviation. *Atmospheric Environment*, *44*(37), 4678–4734. https://doi.org/10.1016/j.atmosenv.2009.06.005

Lin, S. J., & Rood, R. B. (1997). An explicit flux-form semi-Lagrangian shallow-water model on the sphere. *Quarterly Journal of the Royal Meteorological Society*, *123*(544), 2477–2498. https://doi.org/10.1002/qj.49712354416

Liu, X., Ma, P.-L., Wang, H., Tilmes, S., Singh, B., Easter, R. C., et al. (2016). Description and evaluation of a new four-mode version of the Modal Aerosol Module (MAM4) within version 5.3 of the Community Atmosphere Model. *Geoscientific Model Development*, *9*(2), 505–522. https://doi.org/10.5194/gmd-9-505-2016

MacIsaac, B., & Langton, R. (2011). *Gas turbine propulsion systems*. In *AIAA education series*. American Institute of Aeronautics and Astronautics. ISBN 978-1-60086-846-7.

Marsh, D. R., Mills, M. J., Kinnison, D. E., Lamarque, J. F., Calvo, N., & Polvani, L. M. (2013). Climate change from 1850 to 2005 simulated in CESM1 (WACCM). *Journal of Climate*, *26*(19), 7372–7391. https://doi.org/10.1175/JCLI-D-12-00558.1

Matthes, K., Funke, B., Andersson, M. E., Barnard, L., Beer, J., Charbonneau, P., et al. (2017). Solar forcing for CMIP6 (v3.2). *Geoscientific Model Development*, *10*(6), 2247–2302. https://doi.org/10.5194/gmd-10-2247-2017

Meinshausen, M., Vogel, E., Nauels, A., Lorbacher, K., Meinshausen, N., Etheridge, D. M., et al. (2017). Historical greenhouse gas concentrations for climate modelling (CMIP6). *Geoscientific Model Development*, *10*(5), 2057–2116. https://doi.org/10.5194/gmd-10-2057-2017

Mills, M. J., Schmidt, A., Easter, R., Solomon, S., Kinnison, D. E., Ghan, S. J., et al. (2016). Global volcanic aerosol properties derived from emissions, 1990–2014, using CESM1(WACCM). *Journal of Geophysical Research: Atmospheres*, *121*(5), 2332–2348. https://doi.org/10.1002/2015JD024290

Nicolai, L. M., & Carichner, G. E. (2010). *Fundamentals of aircraft and airship design: Volume I—Aircraft design*. In *AIAA education series*. American Institute of Aeronautics and Astronautics. ISBN 978-1-60086-751-4.

Niedzwiecki, R. W. (1992). *Low emissions combustor technology for high-speed civil transport engines*. Langley Research Center, First Annual High-Speed Research Workshop, Part 2. NASA. Retrieved from https://ntrs.nasa.gov/api/citations/19940028975/downloads/19940028975.pdf

Penner, J. E., Lister, D. H., Griggs, D. J., Dokken, D. J., & McFarland, M. (Eds.). (1999). *Aviation and the global atmosphere* (pp. 1–373). Cambridge University Press.

Pitari, G., & Mancini, E. (2001). Climatic impact of future supersonic aircraft: Role of water vapour and ozone feedback on circulation. *Physics and Chemistry of the Earth, Part C: Solar, Terrestrial & Planetary Science*, *26*(8), 571–576. https://doi.org/10.1016/S1464-1917(01)00049-6

Pitari, G., Mancini, E., Rogers, H. L., Dessens, O., Isaksen, I. S. A., & Rognerud, B. (2004). A 3-D model intercomparison of the effects of future Supersonic aircraft on the chemical composition of the stratosphere. In *Proceedings of the 2003 AAC-conference, Friedrichshafen, Germany* (pp. 166–172).

Polvani, L. M., Previdi, M., England, M. R., Chiodo, G., & Smith, K. L. (2020). Substantial twentieth-century Arctic warming caused by ozone-depleting substances. *Nature Climate Change*, *10*(2), 130–133. https://doi.org/10.1038/s41558-019-0677-4

Portmann, R. W., Solomon, S., Garcia, R. R., Thomason, L. W., Poole, L. R., & McCormick, M. P. (1996). Role of aerosol variations in anthropogenic ozone depletion in the polar regions. *Journal of Geophysical Research*, *101*(D17), 22991–23006. https://doi.org/10.1029/96JD02608

Solomon, S., Borrmann, S., Garcia, R. R., Portmann, R., Thomason, L., Poole, L. R., et al. (1997). Heterogeneous chlorine chemistry in the tropopause region. *Journal of Geophysical Research*, *102*(D17), 21411–21429. https://doi.org/10.1029/97JD01525

Solomon, S., Portmann, R. W., Garcia, R. R., Thomason, L. W., Poole, L. R., & McCormick, M. P. (1996). The role of aerosol variations in anthropogenic ozone depletion at northern midlatitudes. *Journal of Geophysical Research*, *101*(D3), 6713–6727. https://doi.org/10.1029/95JD03353

Southwest Research Institute. Numerical Propulsion System Simulation (NPSS). Retrieved from https://www.swri.org/consortia/numerical-propulsion-system-simulation-npss

Spike. (2023). Spike aerospace. Retrieved from https://www.spikeaerospace.com/

Tabazadeh, A., Turco, R. P., & Jacobson, M. Z. (1994). A model for studying the composition and chemical effects of stratospheric aerosols. *Journal of Geophysical Research*, *99*(D6), 12897–12914. https://doi.org/10.1029/94JD00820

Tie, X. X., Brasseur, G., Lin, X., Friedlingstein, P., Granier, C., & Rasch, P. (1994). The impact of high altitude aircraft on the ozone layer in the stratosphere. *Journal of Atmospheric Chemistry*, *18*(2), 103–128. https://doi.org/10.1007/BF00696810

Tilmes, S., Hodzic, A., Emmons, L. K., Mills, M. J., Gettelman, A., Kinnison, D. E., et al. (2019). Climate forcing and trends of organic aerosols in the Community Earth System Model (CESM2). *Journal of Advances in Modeling Earth Systems*, *11*(12), 4323–4351. https://doi.org/10.1029/2019MS001827

Tilmes, S., Lamarque, J. F., Emmons, L. K., Kinnison, D. E., Marsh, D., Garcia, R. R., et al. (2016). Representation of the community Earth system model (CESM1) CAM4-chem within the chemistry-climate model initiative (CCMI). *Geoscientific Model Development*, *9*(5), 1853–1890. https://doi.org/10.5194/gmd-9-1853-2016

Tong, M. T., & Naylor, B. A. (2008). An object-oriented computer code for aircraft engine weight estimation. In *Proceedings of the ASME Turbo Expo* (Vol. 1, pp. 1–7). No. December. https://doi.org/10.1115/GT2008-50062

Trenberth, K. E., & Smith, L. (2005). The mass of the atmosphere: A constraint on global analyses. *Journal of Climate*, *18*(6), 864–875. https://doi.org/10.1175/JCLI-3299.1

Wang, Y., & Huang, Y. (2020). Stratospheric radiative feedback limited by the tropospheric influence in global warming. *Climate Dynamics*, *55*(9), 2343–2350. https://doi.org/10.1007/s00382-020-05390-4

Wang, Y., Logan, J. A., & Jacob, D. J. (1998). Global simulation of tropospheric O3-NO x-hydrocarbon chemistry: 2. Model evaluation and global ozone budget. *Journal of Geophysical Research*, *103*(D9), 10727–10755. https://doi.org/10.1029/98JD00157

Weisenstein, D. K., Ko, M. K., Dyominov, I. G., Pitari, G., Ricciardulli, L., Visconti, G., & Bekki, S. (1998). The effects of sulfur emissions from HSCT aircraft: A 2-D model intercomparison. *Journal of Geophysical Research*, *103*(D1), 1527–1547. https://doi.org/10.1029/97JD02930

Wells, D. P., Horvath, B. L., & McCullers, L. A. (2017). The flight optimization system weight estimation method. NASA Technical Memorandum 219627 (Vol. *TM-2017-21*). No. June.

World Meteorological Organization (WMO). (2018). Scientific assessment of ozone depletion: 2018. World Meteorological Organization, Global Ozone Research and Monitoring Project-Report No. 58. 588 pp.

Zhang, J., Wuebbles, D., Kinnison, D., & Baughcum, S. L. (2021a). Stratospheric ozone and climate forcing sensitivity to cruise altitudes for fleets of potential supersonic transport aircraft. *Journal of Geophysical Research: Atmospheres*, *126*(16), e2021JD034971. https://doi.org/10.1029/2021JD034971

Zhang, J., Wuebbles, D. J., Kinnison, D. E., & Baughcum, S. L. (2021b). Potential impacts of supersonic aircraft emissions on ozone and resulting forcing on climate. *Journal of Geophysical Research: Atmospheres*, *126*(6), e2020JD034130. https://doi.org/10.1029/2020JD034130

References From the Supporting Information

Airlines for America. (2017). A4A passenger airline cost index (PACI).

Boeing. (2019). Commercial market outlook 2019–2038.

FAA. (2015). 2015 inventory as modeled in Aviation Environmental Design Tool (AEDT).

National Aeronautics and Space Administration, & NASA Official: Dan Lockney. Flight Optimization System (FLOPS) Software v.9. NASA Technology Transfer Program.

Niedzwiecki, R. W. (1992). Low emissions combustor technology for high-speed civil transport engines.

Office of the Secretary of Transportation. (September 27, 2016). Revised departmental guidance on valuation of travel time in economic analysis.

WID. (2019). World inequality database (WID). Retrieved from https://wid.world/data/